Dynamic aeroelastic instabilities of fixed-wing aircraft in transonic and supersonic flows using a fully-coupled model

Marcel Ilie¹ and John Havenar² Georgia Southern University, Statesboro, GA, 30458

The aeroelastic phenomena of ONERA M6 wing in transonic and supersonic flight regimes is computationally studied using a fully-coupled aeroelastic approach. The present research concerns the development of a computationally efficient and accurate method for the aeroelastic studies of fixed wing in transonic and supersonic flows. Therefore, we propose a fully-coupled, time-marching aeroelastic approach utilizing an URANS model. The computational studies are carried out to assess the effect of the freestream Mach number and angle of attack on the structural dynamics and stresses developed in the ONERA M6 wing. The studies are carried out for a range of Mach numbers, $M_{\infty} = 0.8 - 1.4$, and angles of attack, $\alpha = \{2^{\circ}, 4^{\circ}, 6^{\circ}\}$. The analysis reveals that the aeroelastic deformation of the wing and induced stress in the wing structure increase with the freestream Mach number.

I. Introduction

Aeroelasticity and the phenomena associated with it present many challenges in modern engineering applications. The effects of aeroelasticity on modern jet aircraft in transonic or supersonic flight can reduce aerodynamic performance and cause dynamic instability throughout the aircraft. Therefore, aeroelastic effects demand consideration during the design process of modern aircraft. By modeling the dynamic aeroelastic response of the wing of a fixed-wing aircraft in transonic and supersonic flight in turbulent flow at a range of angles of attack and Mach numbers, an understanding of the interdependency of the wing structure and the enveloping fluid continuum may be developed.

Flutter is an aeroelastic phenomena of primary concern in the transonic regime due to its ability to quickly damage airframes, fatigue aircraft structures, and lead to a reduction in control surface effectiveness over a relatively short period of time. Consequently, it is given much attention in the aircraft design process. The dynamic instability of flutter is made difficult to predict due to the inherent nonlinearity of transonic flows. Frequency based solutions have demonstrated great effectiveness in predicting flutter, but do not provide the same insights into the fluid dynamics of the flow enveloping the aircraft structure as methods such as computational fluid dynamics (CFD). The parametric analysis of the present work consists of transient aeroelastic simulations which include instances of sudden self-oscillation in the transonic regime, leading to compounding stress throughout the wing structure and oscillation in the lift and drag coefficients.

Computational approaches to modeling aeroelastic systems often utilize two separate solvers: a computational fluid dynamics solver to compute the fluid field with a finite volume method (FVM) or finite difference method (FDM) and a finite element analysis (FEA) solver employing a finite element method (FEM) to compute the structural dynamics of the system. These two solvers are then coupled together with a data passing service which maps force and displacement data between corresponding surfaces in the fluid and structural domains in the CFD and FEA solvers, respectively.

The present work utilizes an explicitly coupled approach which uses a single solver engine comprised of two sub-models. Explicitly coupled aeroelastic models have benefits with regards to both the computational implementation of the aeroelastic model as well as from the aero-structural dynamics perspective. By using a single solver with one sub-model for the fluid flow and another for the structural dynamics, computational overhead is reduced by eliminating the need for a coupling service, as is required by solutions which use two isolated solvers in a staggered, implicitly coupled approach. By modeling the wing structure and the fluid continuum as a single system and computing the fluid and structural dynamics with an implicit time-marching scheme, stable aeroelastic solutions may be found in a single

¹ Assistant Professor, Department of Mechanical Engineering

² Undergraduate Student, Department of Mechanical Engineering

timestep iteration loop, rather than requiring that each solver re-compute the timestep until convergence is reached in the relevant properties.

Unsteady Reynolds-averaged Navier-Stokes (URANS) models have found widespread use in turbulent external aerodynamics applications because of their ability to provide suitable quality results while being computationally efficient relevant to other methods such as large eddy simulation (LES), detached eddy simulation (DES), and scale-adaptive simulation (SAS). Therefore, the present work will use a URANS model to compute the turbulent fluid dynamics of the transonic and supersonic flow regimes studied.

The wing geometry studied is the ONERA M6 wing, which has become a hallmark of transonic CFD validation cases due to the robust experimental pressure data available. To verify the ability of the CFD model to be used in the aeroelastic analyses to accurately model transonic turbulent flow, the surface pressure at multiple span stations on the wing was compared to experimental data for multiple angles of attack and Mach number [1]. The pressure coefficient data from the CFD model and the experimental data compared favorably.

A primary goal of this work is to model the dynamic aeroelastic response of a swept wing in transonic and supersonic flow regimes. The deformation of the wing and the resulting stress throughout the wing structure will be studied and are hypothesized to increase with the angle of attack and Mach number. Sensitivity to dynamic aeroelastic instability in the transonic regime such as undamped self-oscillation is modeled. Additionally, this work serves to strengthen the continually growing body of literature making use of commercial codes to computationally study increasingly complex aeroelastic systems.

II. Computational method and models

Figure 1a presents the details of the ONERA M6 wing. Figure 1b presents the details of the computational domain for the fluid and structure.

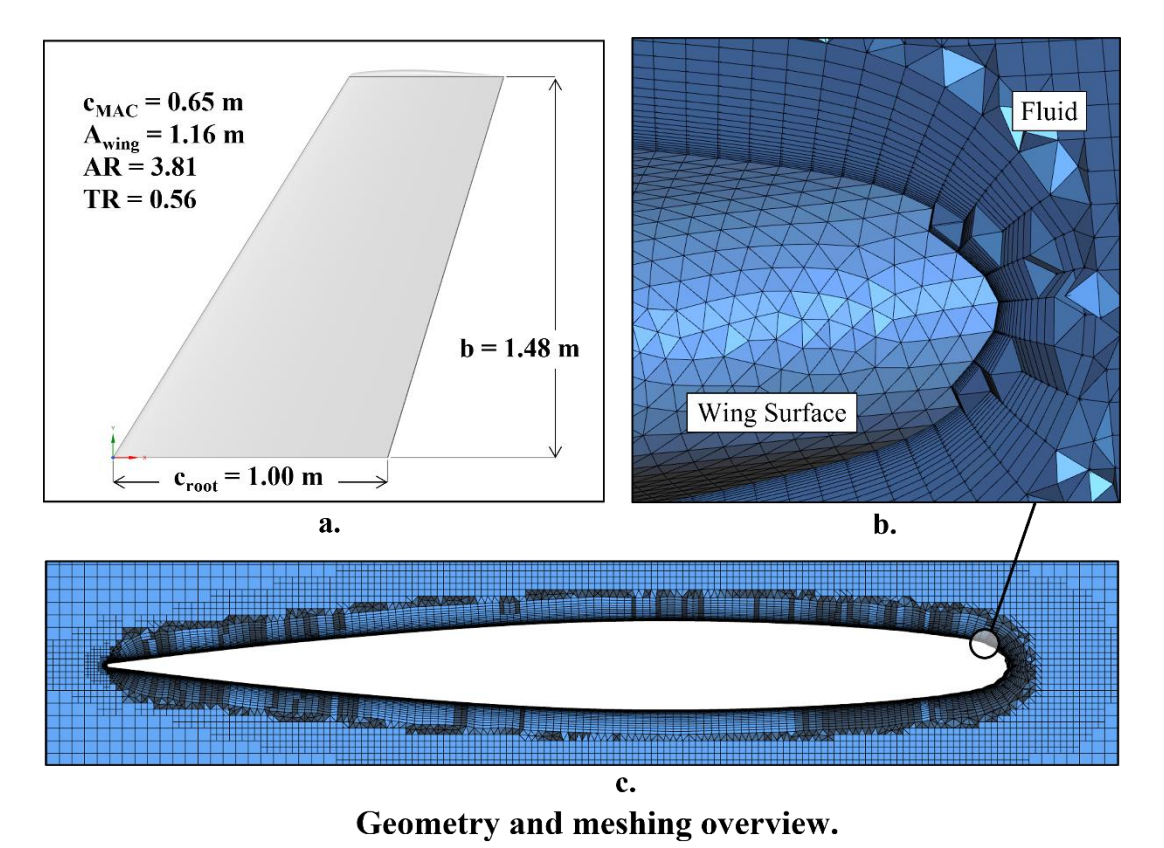


Figure 1. Wing and mesh details

In the present work, an unsteady Reynolds-averaged model is used for the computation of the turbulent flow field enveloping the wing and a linearly elastic structural dynamics method is utilized for the deformation of the wing structure.

The fluid domain was discretized using an unstructured polyhedral meshing scheme with volume refinement near the wing geometry for resolution of wake vorticity [1]. Prism layers were extruded as shown in Fig. 1b from the wing surface mesh to resolve the turbulent boundary layer. The wing structure was meshed with a quadratic tetrahedral scheme with surface sizing equivalent to that of the wing surface in the fluid continuum. The computational fluid domain consists of 4.9 million cells and 20.6 million nodes.

The freestream Mach number was varied between 0.80 and 1.40. A time step of 5×10^5 seconds was selected for the analyses. The turbulent flow field was computed using a finite volume method Navier-Stokes equation solver with the unsteady k- ω SST viscous model, a two-equation eddy-viscosity model capable of accurate prediction of flows with strong adverse pressure gradients and pronounced turbulence features, namely separation and reattachment [2-4]. The k- ω SST model was additionally selected for its promise in transonic buffet prediction when implemented in its unsteady formulation [5].

Within the k- ω SST model, the equations for turbulent kinetic energy and the turbulent dissipation rate are expressed in the conservation form as given by Eq. (1) and Eq. (2), respectively.

$$\frac{\partial(\rho k)}{\partial t} + \frac{\partial(\rho U_i k)}{\partial x_i} = \tilde{P}_k - \beta^* \rho k \omega + \frac{\partial}{\partial x_i} \left[(\mu + \sigma_k \mu_t) \frac{\partial k}{\partial x_i} \right]$$
(1)

$$\frac{\partial(\rho\omega)}{\partial t} + \frac{\partial(\rho U_i\omega)}{\partial x_i} = \alpha\rho S^2 - \beta\rho\omega^2 + \frac{\partial}{\partial x_i} \left[(\mu + \sigma_\omega \mu_i) \frac{\partial\omega}{\partial x_i} \right] + 2(1 - F_1)\rho\sigma_{w2} \frac{1}{\omega} \frac{\partial k}{\partial x_i} \frac{\partial\omega}{\partial x_i}$$
(2)

To avoid instabilities stemming from freestream turbulent parameters, the model uses blending function given by Eq. (3) to transition from the k- ω formulation in the boundary layer to a k- ε model behavior in the freestream flow, where $CD_{k\omega}$ as expressed in Eq. (4) is the positive component of the cross-diffusion term of the turbulent dissipation equation in Eq. (2).

$$F_{1} = \tanh \left\{ \left\{ \min \left[\max \left(\frac{\sqrt{k}}{\beta^{*} \omega y}, \frac{500v}{y^{2} \omega} \right), \frac{4\rho \sigma_{\omega 2} k}{C D_{k \omega} y^{2}} \right] \right\}^{4} \right\}$$
 (3)

$$CD_{kw} = max \left(2\rho \sigma_{\omega 2} \frac{1}{\omega} \frac{\partial k}{\partial x_i} \frac{\partial \omega}{\partial x_i}, 10^{-10} \right)$$
 (4)

The kinematic eddy viscosity, v_t , is given in Eq. (5) and utilizes an additional blending function, F_2 , to scale the vorticity magnitude. The second blending function is given in Eq. (6).

$$v_t = \frac{a_1 k}{max(a_1 \omega, SF_2)} \tag{5}$$

$$F_2 = \tanh\left[\left[max\left(\frac{2\sqrt{k}}{\beta^*\omega y}, \frac{500\nu}{y^2\omega}\right)\right]^2\right]$$
 (6)

To prevent undo excess turbulence in stagnation regions, the turbulence production, P_k , as expressed in Eq. (7), is limited according to the criteria in Eq. (7).

$$P_k = \mu_t \frac{\partial U_i}{\partial x_j} \left(\frac{\partial U_i}{\partial x_j} + \frac{\partial U_j}{\partial x_i} \right), \qquad \tilde{P}_k = \min(P_k, 10 \cdot \beta^* \rho k \omega)$$
 (7)

The closure constants are: $\beta^*=0.09$, $\alpha_1=5/9$, $\beta_1=3/40$, $\sigma_{k1}=0.85$, $\sigma_{\omega 1}=0.5$, $\alpha_2=0.44$, $\beta_2=0.0828$, $\sigma_{k2}=1$, $\sigma_{\omega 2}=0.856$. To ensure the proper resolution of turbulent flow structures and their effects on the wing surface loading, all equations were solved to second order accuracy with a bounded second order implicit transient formulation used to govern the global time-marching of the fluid model.

A no-slip wall was used as the wing surface. A pressure far-field boundary with the freestream Mach number, M_{∞} , specified as requisite characteristic information was imposed a radial distance of $r = 30c_r$ from the wing structure [6].

The fluid mesh dynamically adapted to the aeroelastic deformation of the wing structure via a diffusive smoothing method. The diffusive smoothing method used a diffusion coefficient which was a function of a normalized boundary distance in order to shift the burden of mesh motion away from the highly-sensitive near-wall region [7].

The governing Laplace equation for the mesh motion and the formulation of the diffusion coefficient, γ , where $0 \le \alpha \le 2$, are given as Eq. (8).

$$\nabla \cdot (\gamma \nabla \vec{u}) = 0, \qquad \gamma = \frac{1}{d^{\alpha}}$$
 (8)

The wing structure was treated as a linearly elastic structural continuum and the deformation was computed with a finite element method (FEM). The wing structure dynamics were computed the beta-Newmark time-integration algorithm, a single-step time integration algorithm proven effective for the computation of structural dynamics with transient surface loading [8].

III. Results and Discussion

Figure 2 presents the ONERA M6 wing with the interrogation line where the data is collected and analyzed. The interrogation line is located at 20% of the span measured from the hub of the blade.

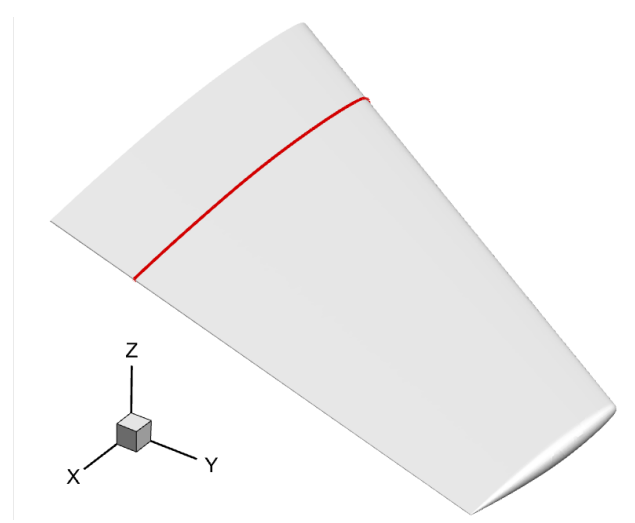


Figure 2. ONERA M6 wing (interrogation line at 20% of span)

Figure 3 presents the variation of the Mach number with the angle of attack (AoA) for transonic flow regime. The analysis of the Mach umber shows the presence of the shock with the increase of Mach number and angle of attack. Therefore, for a Mach number flow M=0.8, the increase of AoA is associated with the presence of shocks as seen in Figure 3, for M=0.8 and $AoA=6^{\circ}$. On the other hand the effect of the Mach number on the fluid flow can be seen from the flow field analysis for $AoA=2^{\circ}$. Thus, the increase of Mach number generates shocks whose intensities increase with the increase of Mach number. However, there are differences in the behavior of the fluid flow for different Mach numbers. Therefore, for a Mach number M=1, the strongest shocks are anchored at the trailing-edge while expansion waves are observed at the leading-edge. The increase of Mach number to M=1.2 generates a bow shock ahead of the airfoil as seen in Figure 3 for a Mach number M=1.2 and $AoA=2^{\circ}$. Similar trends were observed for the other angles of attack and Mach numbers.

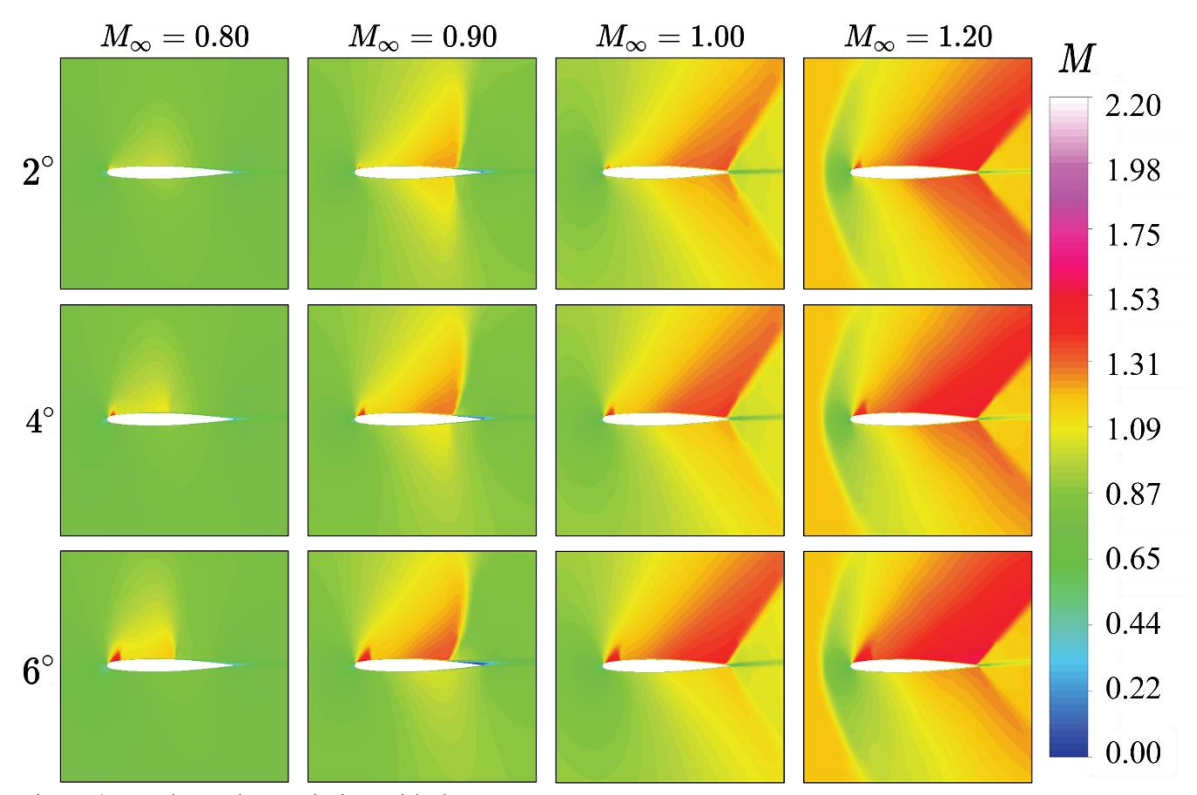


Figure 3. Mach number variation with the AoA

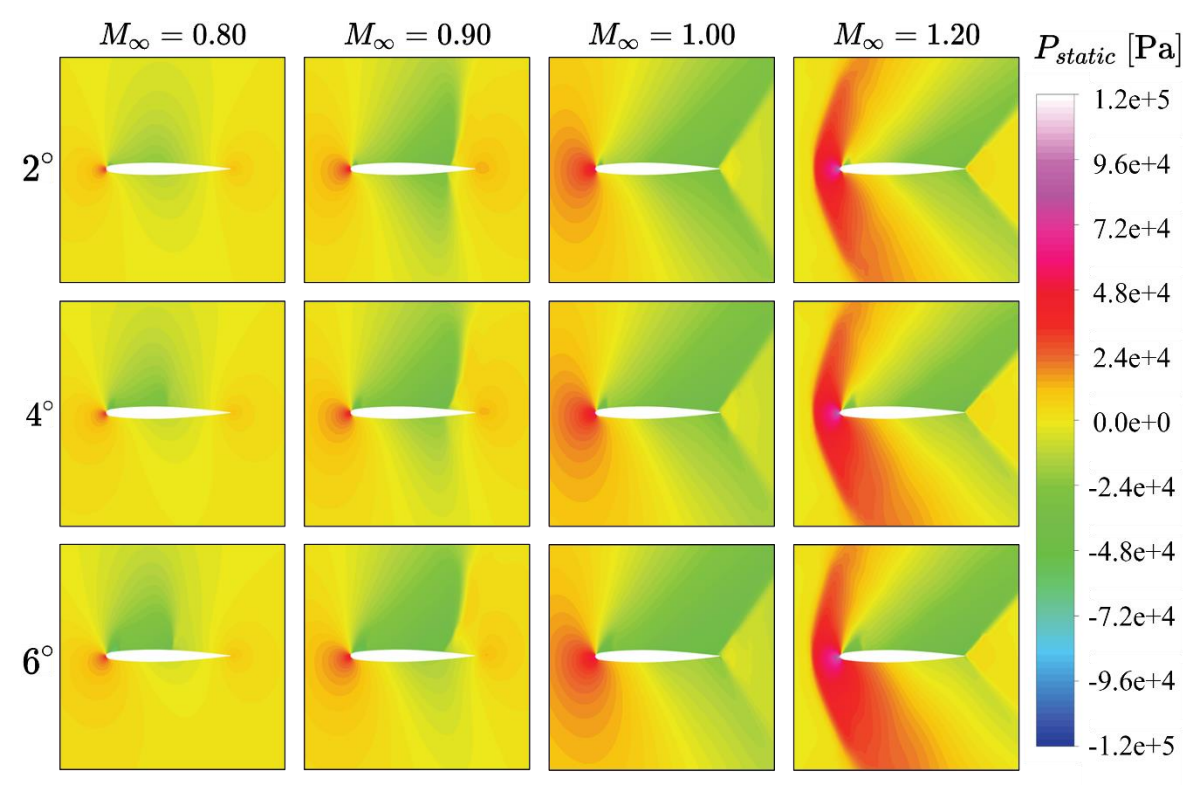


Figure 4. Pressure variation with the Mach number and AoA

Figure 4 presents the pressure variation with the Mach number and angle of attack. The analysis of the pressure field also reveals the presence of the shocks and their increasing strength with the Mach number and angle of attack.

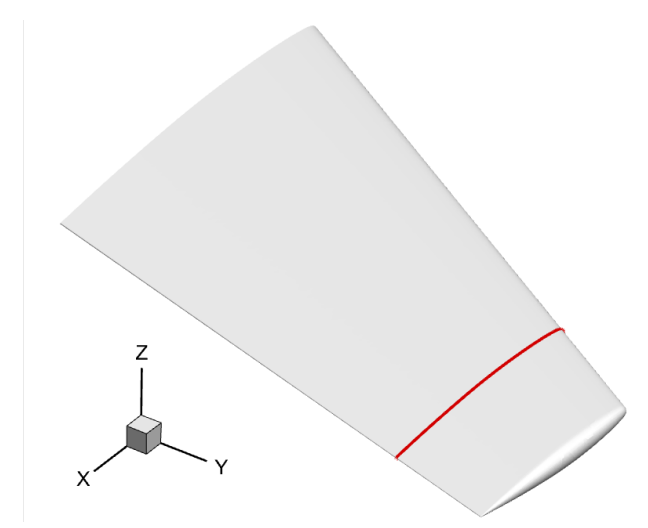


Figure 5. ONERA M6 wing (interrogation line at 80% of span)

Figure 5 presents the ONERA M6 airfoil and interrogation line at 80% span from the hub of the wing. In the following the variation of the Mach number with the angle of attack is presented. Therefore, the analysis of the Mach number at this location is presented in Figure 6. The analysis of the Mach number at this location reveals the flow separation at the upper surface of the wing for $AoA = 6^{0}$ and Mach numbers M=0.8 and M=0.9. The flow separation diminishes with the increase of the Mach number.

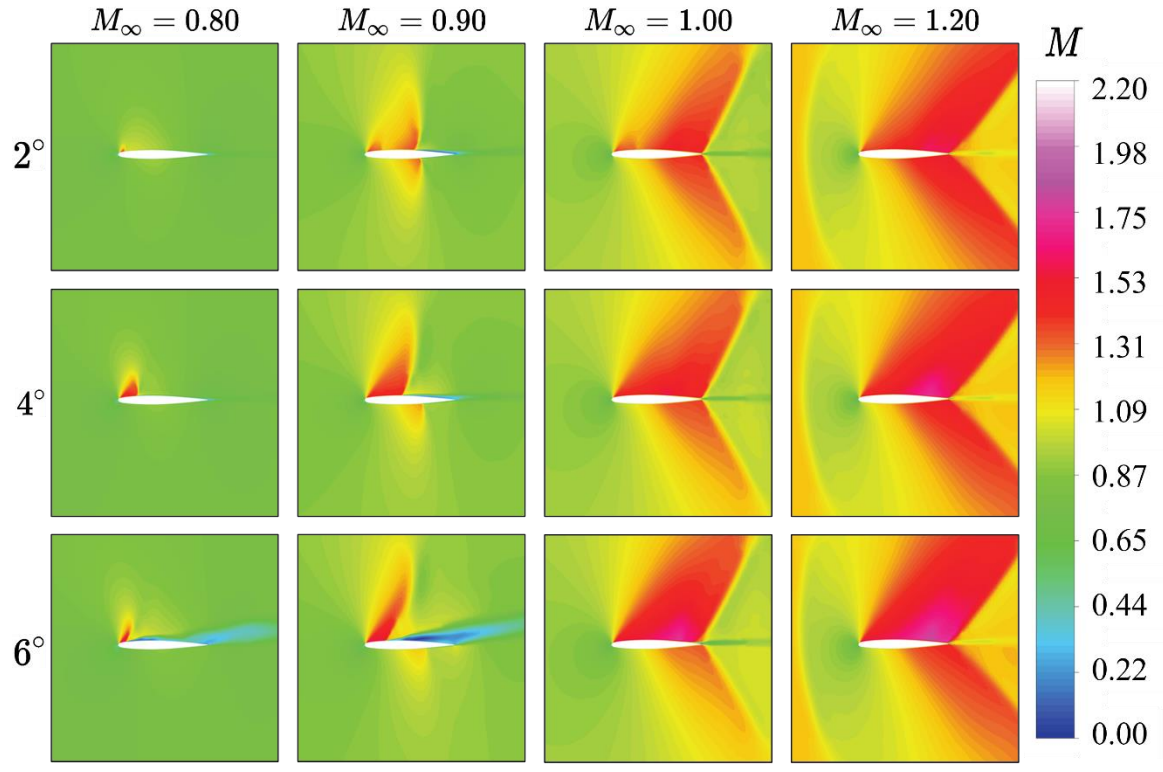


Figure 6. Mach number variation with the AoA

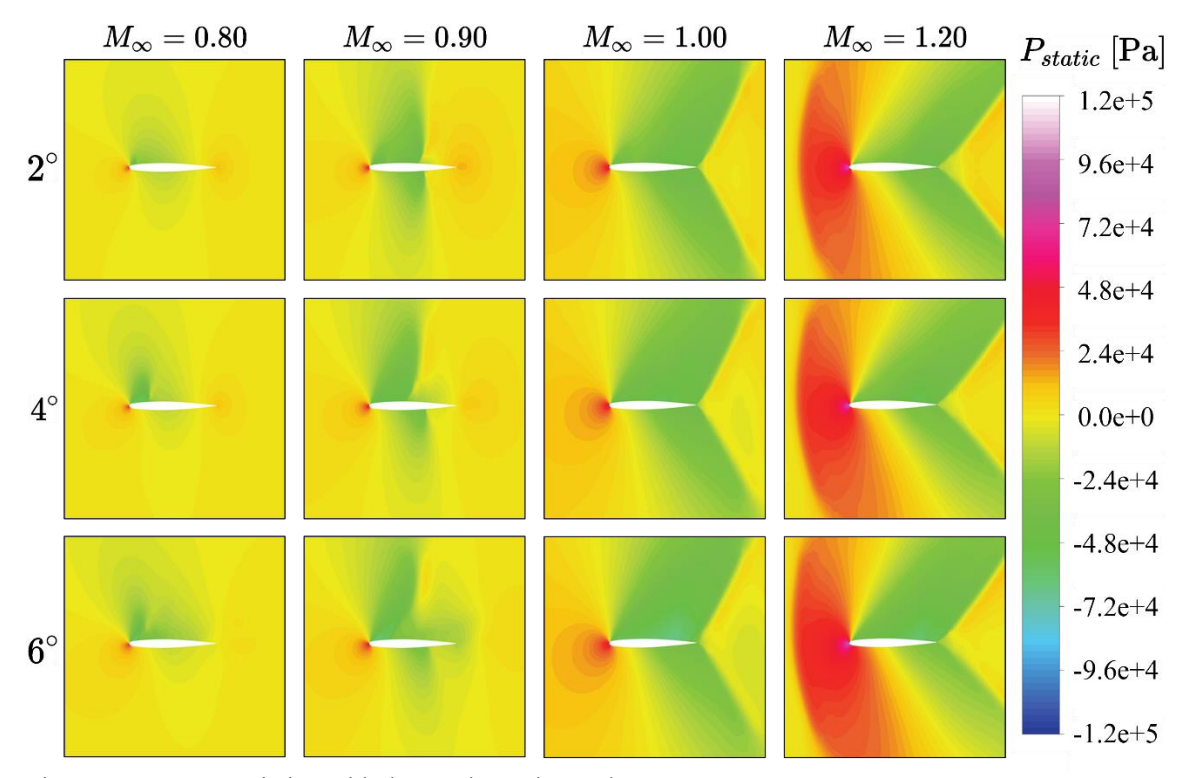


Figure 7. Pressure variation with the Mach number and AoA

Figure 7 presents the pressure variation with the Mach number and angle of attack. The analysis shows that there is a decrease of the pressure in the nearfield of the wing in the region close to the tip of the wing.

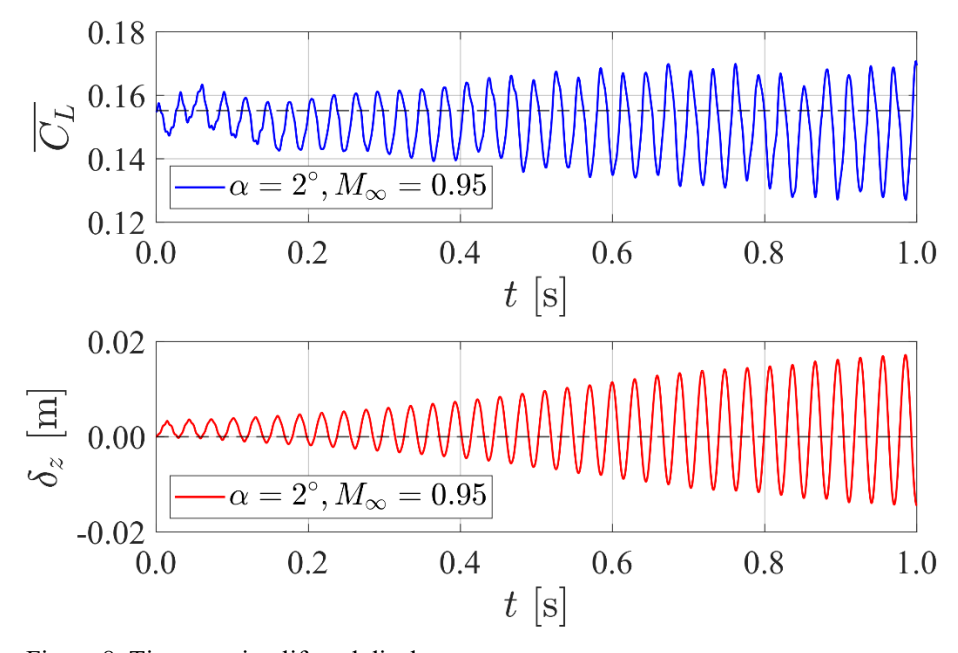


Figure 8. Time-varying lift and displacement

Figure 8 presents the time-varying lift coefficient and wing displacement, for M=0.95 and $AoA = 2^0$. The analysis shows that the lift coefficient oscillations increase with time reaching a steady-state value of about $C_L = 0.15$. The wing displacement oscillations also increases with the lift coefficient.

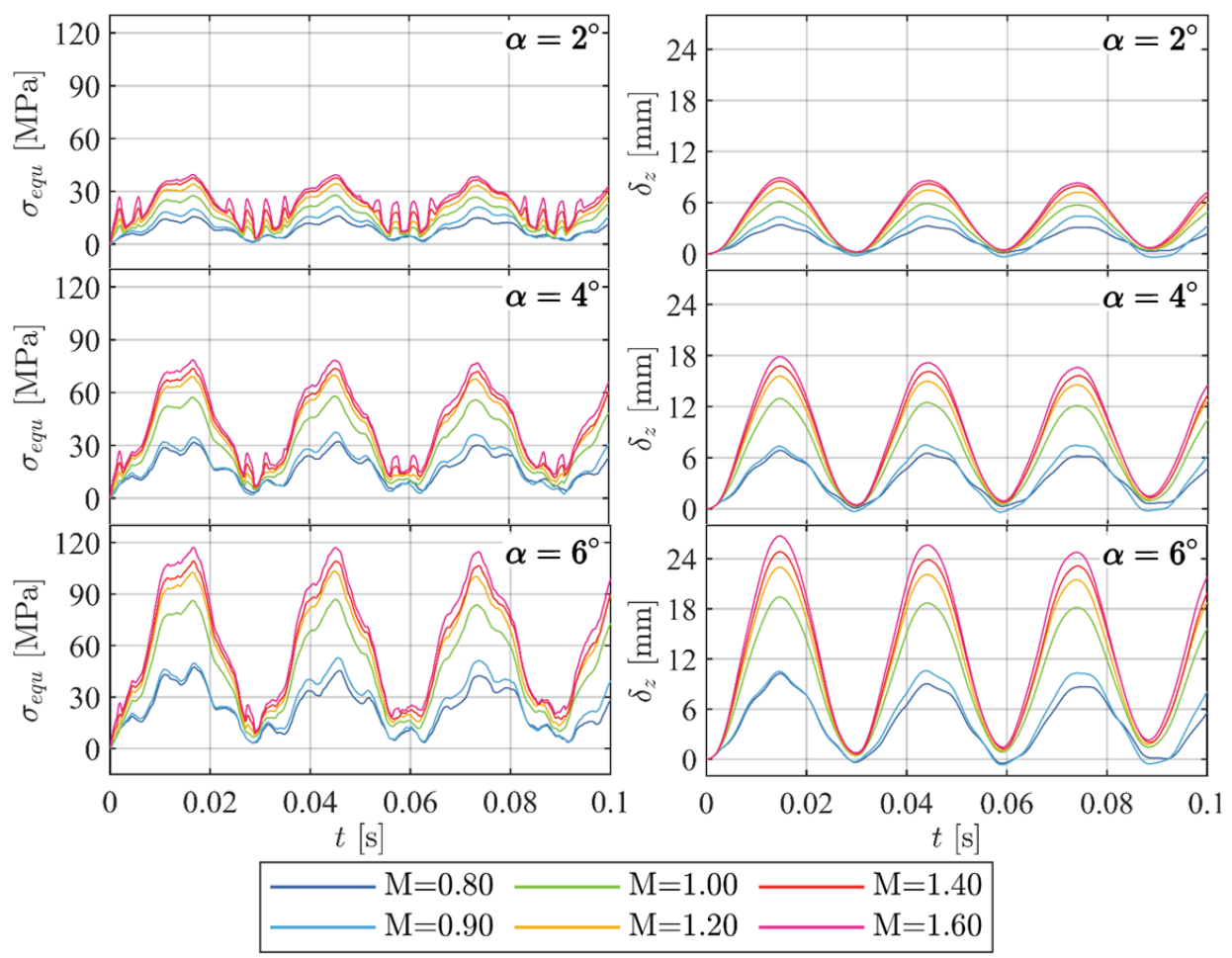


Figure 9. Time variation of the equivalent stress and displacement with the Mach number

Figure 9 presents the time variation of the Mach number and wing displacement with the Mach number. The analysis shows that both the equivalent stresses and wing displacement increase with the Mach number and angle of attack. Figure 10 presents the equivalent stress and wing deformation. The analysis shows the presence of large stresses in the hub region of the wing and displacements at the tip of the wing.

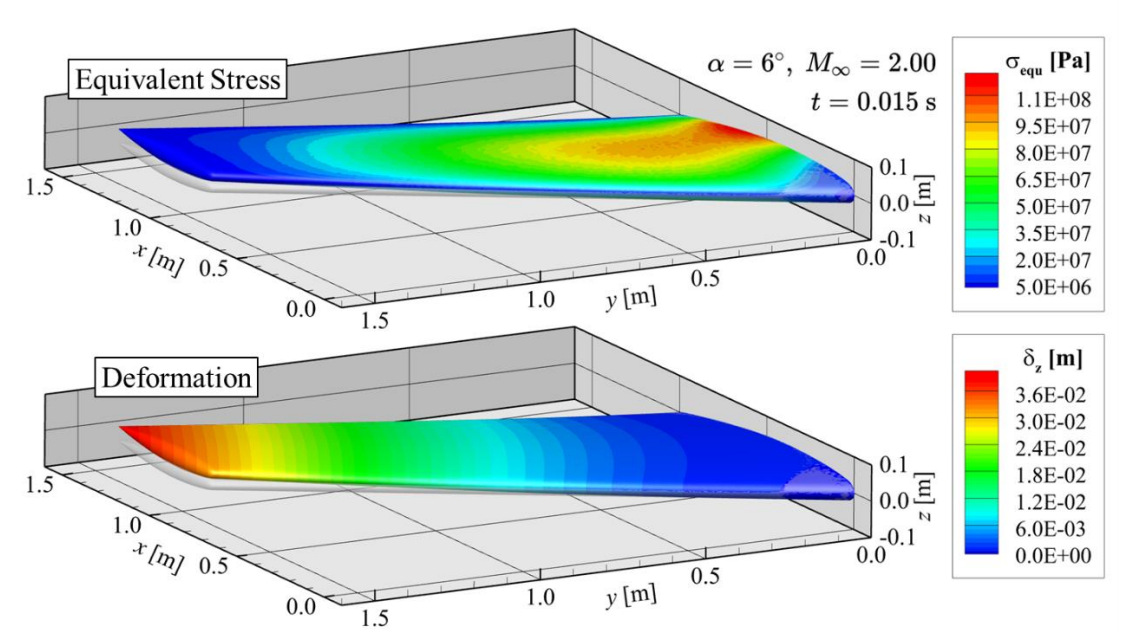


Figure 10. Equivalent stress and displacement

IV. Conclusions

A fully-coupled computational aeroelasticity model is developed for the prediction of the flow field and structural dynamics of swept wing in the transonic and supersonic regimes. Mach number effect on the aeroelasticity phenomena, of the swept wing, is computationally studied using the fully-coupled aeroelastic method. The flow field is computed using the CFD approach using finite-differences, while the structural analysis is performed using the finite-element method. The study reveals the presence of the bow shock in the transonic and supersonic flight regimes. For supersonic flow, shock waves are present at the trailing-edge. The study shows that the pressure on the lower surface of the wing increases with the Mach number. The elastic deformation and stresses, on the wing, increase with the Mach number. The analysis shows that the upper and lower surfaces of the wing experience alternatively, tensions and compressions.

References

- [1] C. Brady. "Boeing 737 Winglets." b373.org.uk. http://www.b737.org.uk/winglets.htm (accessed 2021).
- [2] E. H. Dowell, A Modern Course in Aeroelasticity, 5 ed. (Solid Mechanics and Its Applications). Cham, Switzerland: Springer International Publishing, 2015, p. 700.
- [3] F. R. Menter, "Two-equation eddy-viscosity turbulence models for engineering applications," AIAA Journal, vol. 32, no. 8, pp. 1598-1605, 1994, doi: 10.2514/3.12149.
- [4] N. M. Newmark, "A Method of Computation for Structural Dynamics," Journal of the Engineering Mechanics Division, vol. 85, no. 3, pp. 67-94, 1959, doi: doi:10.1061/JMCEA3.0000098.
- [5] V. Schmitt and F. Charpin, "Pressure distributions on the ONERA M6 wing at transonic Mach numbers," in AGARD AR, 1979, vol. 138, pp. B1-1-B1-44.
- [6] Zore, K., Shah, S., Stokes, J., Sasanapuri, B., and Sharkey, P. "ANSYS CFD Study for High Lift Aircraft Configurations," 2018 Applied Aerodynamics Conference. 2018.

- [7] Menter, F., Kuntz, M., and Langtry, R. B. "Ten years of industrial experience with the SST turbulence model," Heat and Mass Transfer Vol. 4, 2003.
- [8] Menter, F. R. "Two-equation eddy-viscosity turbulence models for engineering applications," AIAA Journal Vol. 32, No. 8, 1994, pp. 1598-1605. doi: 10.2514/3.12149
- [9] Menter, F. "Zonal Two Equation k-w Turbulence Models For Aerodynamic Flows," 23rd Fluid Dynamics, Plasmadynamics, and Lasers Conference. American Institute of Aeronautics and Astronautics, 1993.
- [10] Kumada, K., and Sawada, K. "Improvement in prediction capability of Transonic Buffet on NASA-CRM Using URANS," *54th AIAA Aerospace Sciences Meeting*. 2016.
- [11] Jameson, A. "Aerodynamic design via control theory," *Journal of Scientific Computing* Vol. 3, No. 3, 1988, pp. 233-260.
 - doi: 10.1007/BF01061285
- [12] ANSYS. "Fluent User's Guide." ANSYS, Inc., Canonsburg, PA, 2021, pp. 1581-1582.
- [13] Newmark, N. M. "A Method of Computation for Structural Dynamics," *Journal of the Engineering Mechanics Division* Vol. 85, No. 3, 1959, pp. 67-94.
 - doi: 10.1061/JMCEA3.0000098